

Exceptionally flame-retardant flexible polyurethane foam composites: synergistic effect of the silicone resin/graphene oxide coating

Qian Wu^{1*}, Jincheng Zhang^{1*}, Shengpeng Wang³, Bajin Chen³, Yijun Feng³, Yongbing Pei (✉)^{1,2}, Yue Yan¹, Longcheng Tang¹, Huayu Qiu^{1,2}, Lianbin Wu (✉)^{1,2}

¹ Key Laboratory of Organosilicon Chemistry and Materials Technology of Ministry of Education, Hangzhou Normal University, Hangzhou 311121, China

² Collaborative Innovation Center of Zhejiang Province for Manufacturing of Fluorine Silicon Fine Chemicals and Materials, Hangzhou Normal University, Hangzhou 311121, China

³ Transfar Zhilian Co., Ltd., Hangzhou 311215, China

© Higher Education Press 2020

Abstract A facile strategy was developed to fabricate flexible polyurethane (PU) foam composites with exceptional flame retardancy. The approach involves the incorporation of graphene oxide (GO) into a silicone resin (SiR) solution, which is then deposited onto a PU foam surface via the dip-coating technique and cured. Fourier-transform infrared spectroscopy, scanning electron microscopy, and Raman spectroscopy measurements demonstrated that the SiR and GO were successfully coated onto the PU skeleton and the intrinsic porous structure of the PU foam remained intact. The effects of SiR and GO on the mechanical and thermal stability and flame retardancy of PU composites were evaluated through compression tests, thermogravimetric analysis, vertical combustion tests, and the limiting oxygen index. The measurement results revealed that the composites (PU@SiR-GO) showed superior flame retardancy and thermal and mechanical stability compared to pristine PU or PU coated with SiR alone. The mechanical and thermal stability and the flame-retardant properties of the PU composites were enhanced significantly with increasing GO content. Based on the composition, microstructure, and surface morphology of PU@SiR-GO composites before and after combustion tests, a possible flame-retardance mechanism is proposed. This work provides a simple and effective strategy for fabricating flame-

retardant composites with improved mechanical performance.

Keywords flame retardancy, flexible polyurethane foam, graphene oxide, silicone resin

1 Introduction

Polymeric materials, such as porous flexible polyurethane (PU) foam, have been widely used in daily life. Specific examples include household, automotive, and insulation applications due to the excellent elastic, acoustic, and thermal insulation properties of these materials [1–3]. Unfortunately, most of these polymers are combustible materials. For example, PU foam is easily ignited by small fire sources (a flame, cigarette, etc.). It can combust completely in several seconds, accompanied by continuous dripping and quick flame self-propagation. During the combustion process, PU foam generates substantial quantities of toxic fumes and molten products with a high rate of heat release [4,5]. This greatly increases fire hazards that threaten the security of human lives and property. With increasingly strict standards and growing demands on fire safety regulations and environment protection, it is of great interest to improve the flame retardancy of combustible polymeric foam [6,7].

To reduce the flammability of polymers, two typical strategies have been developed [8]. One method is to incorporate flame retardants into polymers [9]. These flame retardants mainly include phosphorus-nitrogen flame retardants [10,11] and other nano-materials such as

Received May 25, 2020; accepted July 10, 2020

E-mails: wulianbin@hznu.edu.cn (Wu L);
peiyongbing@hznu.edu.cn (Pei Y)

*These authors contributed equally to this work.

aluminum nano-particles [12], aluminum hypophosphite [13], and aluminum diethylphosphinate (ADP) [14]. Due to the excellent flame retardancy of these materials, incorporating these flame retardants into combustible polymers can interfere with polymer ignition, decomposition, and flame spreading. Once the polymer catches fire, combustion can be retarded by the combination of physical and chemical actions, such as the formation of a protective layer, degradation of additives to a cool environmental temperature [15], and dilution of gas mixtures to a lower ignition limit [16]. This approach has been widely used to improve the flame retardancy of polymer materials. However, a relatively high content of flame-retardant is usually required to achieve the desired flame retardancy, which could result in the sacrifice of mechanical properties of the polymer, such as tensile or flexural strength. For example, Wang et al. prepared flame-retardant and flexible PU foam, by a free-foaming method with ADP as additives, and found that when the ADP loading was 20%, the peak heat release rate and the total heat release of the resultant PU foam was reduced by 35% and 33%, respectively [14].

Another method to improve flame retardancy is to construct a flame-retardant coating on the surface of polymers [17–19]. The advantage of this method is easy processing on the foam surface and an ignorable influence on the intrinsic properties of the polymer [19]. Recently, a variety of non-combustible inorganic and/or difficult-to-combust organic materials were utilized as flame-retardant coatings. These materials included metal compounds [5,20,21], clay [22,23], nitrogen organic compounds [24], sulfur-nitrogen organic compounds [25], sodium alginate [26,27], carbon black [28], montmorillonite [29], carbon nano-tubes [30], graphene oxide (GO) [31], silicone resin (SiR) [32], aerogels [33], and nano-fibers [34]. For example, Chen et al. constructed polymer-clay coatings on flexible PU foam with a nano-brick wall structure and found a lower clay content was more efficient to reduce the flammability of the PU foam [35].

Of the methods to construct protective coatings on flexible PU foam, the layer-by-layer method has been widely used due to its ease of manipulation. For example, Hai et al. deposited silica aerogel and sodium alginate on the skeleton surface of PU foam via layer-by-layer assembly. The resulting PU foam reached the V-0 level of the vertical combustion test [36]. Lin et al. prepared MXene/chitosan flexible nano-coatings on PU foam by the layer-by-layer method, and the coating significantly reduced the flammability and smoke release of PU foam. At the same time, the adverse effects on the inherent performance of PU were minimized [37]. Furthermore, clay and carbon nano-tube based coatings showed a synergistic effect in reducing the flammability of flexible PU foam [38].

The improvement of flame retardancy and smoke suppression performance of coated PU foam has been

attributed to the high quality of the protective barrier of the hybrid coating. Among the nano-materials used in coatings, GO has commonly been complexed with other organic/inorganic materials to create a hybrid, flame-retardant coating on PU foam due to its high specific surface area and physical barrier [39,40]. For example, Maddalena et al. constructed binary GO/chitosan coatings and found it capable of improving the flame retardancy of open-cell PU foams [41]. In addition, Lu et al. fabricated a ternary GO, chitosan, and alginate coating on the surface of PU foam through the layer-by-layer method. The flame retardancy of these PU foam composites were significantly improved after a ten-cycle layer-by-layer assembly [31]. Although these layer-by-layer assembled coatings have proven to be effective at improving the flame retardancy of PU foam, most of the abovementioned surface coating fabrication processes are time-consuming. They involve many steps, which greatly restricts the scale-up preparation of flame-retardant PU foam composites.

Due to the higher bonding energy of the Si–O bond ($460.5 \text{ kJ}\cdot\text{mol}^{-1}$) relative to C–C ($304.0 \text{ kJ}\cdot\text{mol}^{-1}$) and C–O ($358.0 \text{ kJ}\cdot\text{mol}^{-1}$) bonds, organosilicone, such as polyhedral oligomeric silsesquioxane [42], and organosilicon polymers, such as SiR, have gained tremendous attention and have been used to reduce the flammability of PU foams due to their excellent thermal stability at temperatures exceeding $350 \text{ }^\circ\text{C}$ [43,44]. As an environmentally friendly flame-retardant, SiR has displayed a slow combustion rating, low heat release rate (HRR), minimal toxic gas emission, and low yield of carbon monoxide during the combustion process [45,46]. In our previous work, we developed a strategy for fabricating highly flame-retardant and flexible PU foam composites by coating with SiR via a facile dip-coating process [32]. This multilayer flame-retardant coating can significantly improve the flame retardancy of PU foam. However, only when the weight of coated SiR was 4.8 times that of the PU foam it was sufficiently effective to reduce the flammability of the PU foam; the flame could be completely extinguished 30 s after ignition. Moreover, the density of PU foam drastically increased from $0.024 \text{ g}\cdot\text{cm}^{-3}$ to $0.140 \text{ g}\cdot\text{cm}^{-3}$, before and after coating with SiR. The increased density may cause problems, such as difficult transport and scarification of mechanical properties, which would restrict the application of this method. To our knowledge, little progress had been made in fabricating flame-retardant and flexible PU foam using a simple strategy in which no time-consuming fabrication process is involved with no adverse effects.

Herein, based on the excellent thermal stability of SiR and previous work in which a large amount of SiR was required to coat PU foam, but with a time-consuming process and weight-gain [32], we aimed to develop a facile and fast strategy to prepare a flame-retardant and flexible PU foam. In this article, we incorporate GO nano-sheets into a SiR solution then deposit the hybrid GO-SiR coating onto the PU foam surface via the dip-coating technique,

resulting in decreased weight-gain, to achieve high flame retardancy. The microstructure and surface morphology of the PU foam composites were characterized, and the effects of SiR and GO on the flame retardancy and mechanical and thermal stability of PU composites were investigated. The results indicate that the SiR-GO coating exhibited a synergistic effect on improving the flame retardancy of PU foam composites, and the resulting composites (PU@SiR-GO) show superior thermal stability compared to PU starting materials or PU coated with SiR alone. The PU@SiR-GO exhibits a more stable thermal stability with increasing GO content. Additionally, a possible flame-retardant mechanism is proposed based on the microstructure and composition analysis before and after combustion tests.

2 Experimental

2.1 Materials

Natural graphite powder (325 mesh, 99 wt-%) was obtained from Qingdao OER graphite Co., Ltd. Methyltrimethoxysilane ((CH₃)Si(OCH₃)₃, 98 wt-%), dimethoxydiphenylsilane ((C₆H₅)₂Si(OCH₃)₂, 98 wt-%), diethoxydimethylsilane ((CH₃)₂Si(OC₂H₅)₂, 98%), phenyltrimethoxysilane ((C₆H₅)Si(OCH₃)₃, 98%), and ethyl alcohol (95%) were purchased from Sinopharm Chemical Reagent Co., Ltd. Concentrated sulfuric acid (H₂SO₄, ≥95%), phosphorus pentoxide (P₂O₅, 98 wt-%), potassium peroxydisulfate (K₂S₂O₈, 98 wt-%), potassium permanganate (KMnO₄, 98%), hydrogen peroxide (H₂O₂, 30 vol-%), hydrochloric acid (HCl, 35 wt-%), and double amino-terminated polyetheramine (D230, molecular weight approximately 230) were obtained from Sinopharm Chemical Reagent Co., Ltd. (China). PU foam (0.025 g·cm⁻³, polyester-type) was provided by Zhejiang Hangzhou Guangsheng Foam Plastic Company.

2.2 Preparation of GO and SiR

First, GO was prepared by the oxidation of graphite powder using the modified Hummers' method [47]. SiR was prepared through co-hydrolysis and condensation. Diethoxydimethylsilane (160 g), dimethoxydiphenylsilane (64 g), phenyltrimethoxysilane (100 g), methyltrimethoxysilane (30 g), ethanol (250 g), and hydrochloric acid solution (2 vol-%) were added into a 1000 mL, three-necked, round-bottom flask equipped with a thermometer and a reflux condenser. The mixture was heated to 65 °C – 70 °C, then 120 g of deionized water was slowly added while stirring. After the hydrolysis was completed, the NaHCO₃ solution was added to neutralize the solution until the pH value of the mixture was neutral. Finally, the mixture was filtered and the filtrate was heated to 100 °C under vacuum for 1 h to remove the solvent. A SiR-

containing R/Si ratio of 1.65 (R indicates the total mole of methyl and phenyl groups, and Si indicates the mole of Si element) was obtained.

2.3 Preparation of PU@SiR-GO foam composites

The preparation process of PU@SiR-GO foam composites is illustrated in Fig. 1(a). First, SiR (19.8 g), GO nano-sheets (0.20 g), ethanol (100 g), and the cross-linking agent double amino-terminated polyetheramine (D230, 0.2 g) were mixed under high-speed stirring (2000 r·min⁻¹) for 20 min then sonication for 10 min. Subsequently, the PU foam was fully immersed in the GO and SiR mixture for 15 min under vacuum, and the sample was then centrifuged at 600 r·min⁻¹ for 5 min prior to curing at 90 °C for 4 h. The above procedures were repeated until the coated SiR-GO weight was approximately twice that of the pristine PU foam. The obtained foam composites were designated as PU@SiR-GO 1.00%. The designation of foam composites with different GO to SiR ratios is given by PU@SiR-GO X wt-%, with X representing the weight ratio of GO to SiR components. The PU@SiR-GO 0 wt-% (i.e., without adding GO), PU@SiR-GO 0.25%, and PU@SiR-GO 0.50% samples were obtained using the same method while adjusting GO weight to obtain the desired wt-% ratio of GO to SiR.

2.4 Characterization methods

The morphological structures of PU and PU foam composites before and after combustion were investigated using scanning electron microscopy (SEM, SIGMA 500). Fourier transform infrared (FTIR) spectra were obtained on a Nicolet 7000 FTIR (Nicolet Instrument Company, USA) in the range of 4000 to 600 cm⁻¹. Thermogravimetric analysis (TGA) was employed using a TA Instruments Q5000 under a nitrogen atmosphere and at a linear heating rate of 10 °C·min⁻¹ from 25 °C to 800 °C. Compression tests were performed using an AMETEK Ls 100Plus at a compression speed of 1.0 mm·min⁻¹ at 25 °C with a sample size of 20.0 mm length × 20.0 mm width × 10.0 mm thickness. Flammability was characterized by the vertical burning test. Before testing, the specimens were conditioned at 25 °C ± 1 °C and 50% ± 2% relative humidity for 72 h. The specimen dimensions were 50 ± 2 mm length × 25 ± 2 mm width × 10 ± 0.5 mm thickness and each specimen was fixed approximately vertical. Limiting oxygen index (LOI) values were measured by a JF-3 oxygen index meter (Jingning Analysis Instrument Company, China) according to the test standard of ASTM D2863-97 with samples having dimensions of 100 mm length × 10 mm width ± 10 mm thickness. A cone calorimeter was employed to evaluate the flame retardancy of PU and PU composites according to the test standard of ISO 5660-1; each sample had dimensions of 100 mm length × 100 mm width × 10 mm thickness. The samples

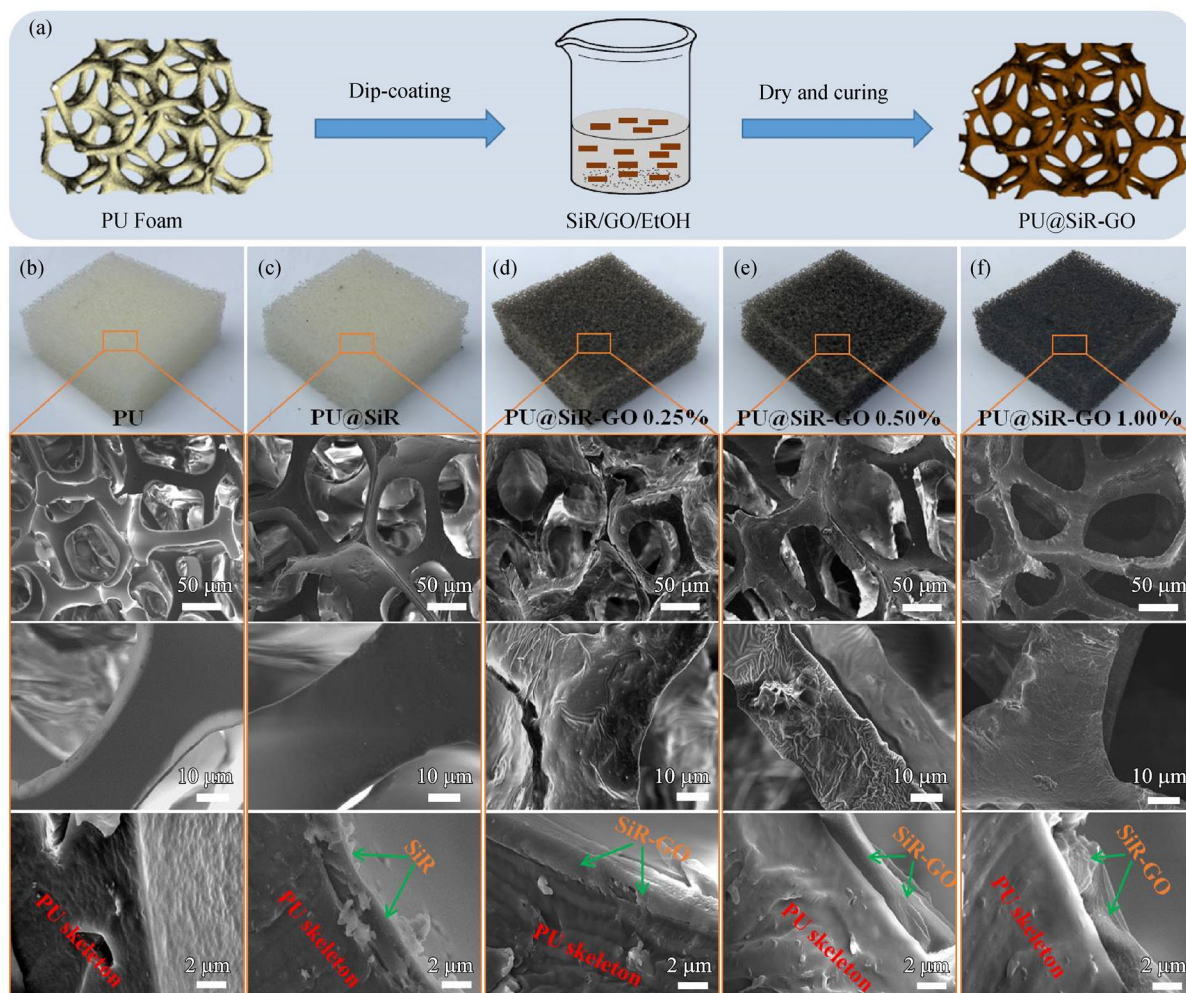


Fig. 1 (a) Preparation process of PU@SiR-GO foam composites. Digital and SEM images of (b) pristine PU, (c) PU@SiR, (d) PU@SiR-GO 0.25%, (e) PU@SiR-GO 0.50%, and (f) PU@SiR-GO 1.00%.

were wrapped with aluminum foil and mounted into a heavy metal container. The container was horizontally exposed to a heat flux of $35 \text{ kW} \cdot \text{m}^{-2}$ and tests were repeated at least three times for each sample. Raman spectra were recorded using a SENTERRA Micro Raman Spectrometer (Bruker Instruments, Germany) with a 633 nm He-Ne laser beam from 200 to 4000 cm^{-1} .

3 Results and discussion

3.1 Microstructure and composition analysis

Digital photos of PU and PU composites, reflecting their macroscopic evolution during the PU foam composite preparation process, are shown in Figs. 1(b–f). The pristine PU sponge is white in appearance; thus, the PU@SiR keeps its original color due to the transparency of the SiR coating. After the incorporation of GO, all the samples of

PU@SiR-GO 0.25%, PU@SiR-GO 0.50%, and PU@SiR-GO 1.00% appear dark. The PU composite color gradually becomes darker with the increase in GO content. This is due to the dark appearance of GO nano-sheets and demonstrates that GO has coated the surface of the PU.

Additionally, SEM images of the pristine PU and PU foam composites are shown in Figs. 1(b–f). As shown in Fig. 1(b), the pristine PU foam skeleton has a clear structure. The skeleton surface is smooth and crack-free, while the edge is lighter than the inner region. The SEM images of PU@SiR in Fig. 1(c) show that the foam skeleton structure is still clear after dip-coating in SiR. Both the pristine PU and PU@SiR skeleton surfaces are smooth and crack-free, but a two-layered structure is only observed in the magnification image of PU@SiR. One layer is the PU foam skeleton, and the other layer is the SiR coating. Moreover, it can be observed that the thickness of the SiR coating is approximately $2 \mu\text{m}$. SEM images of PU@SiR-GO 0.25% are shown in Fig. 1(d). It can be

observed that the porous structure of PU composites remains intact with approximately a 2 μm thick layer on the skeleton surface. However, the skeleton surface grows rougher, with many pleats arising compared to the smooth surface in Fig. 1(c). This phenomenon is likely due to the incorporation of GO and its wrinkling effect, which is consistent with reported work [31]. Moreover, when the GO content is increased to 0.50%, and 1.00%, the porous structure of PU@SiR-GO 0.50% (Fig. 1(c)) and PU@SiR-GO 1.00% (Fig. 1(f)) remain intact and free of any noticeable pore blocking. It is noted that, in the highest magnification images, the skeleton surfaces of these two PU composites became rougher due to the GO wrinkling effect.

To further demonstrate the incorporation of the GO-SiR coating on the surface of the PU, the FTIR spectra of PU and PU foam composites were measured, and the results are shown in Fig. S1 (cf. Electronic Supplementary Material, ESM). For the PU foam, the band at 3280 cm^{-1} matches the stretching vibration of the N-H bond, and the bands at 3330 and 1220 cm^{-1} correspond to the deformation stretching vibration of the N-H and stretching vibration of the N-C band, respectively. The bands at 2980 and 2880 cm^{-1} are assigned to the stretching vibration of the C-H band. The band at 1718 cm^{-1} corresponds to the stretching vibration of the C=O bond, and the bands at 1220 and 1094 cm^{-1} correspond to the stretching vibration

of the C-O-C band of an aliphatic compound and stretching vibration of the C-O band of aromatic compounds, respectively. For PU@SiR, the most distinct difference with pristine PU is the new occurrence of bands at 1020 and 790 cm^{-1} , which can be assigned to the stretching vibration of the Si-O-Si bond and the Si-C band, respectively. The presence of Si-O-Si and Si-C bands prove that SiR has been successfully prepared and deposited onto the PU foam surface. For the samples of PU@SiR-GO 0.25%, PU@SiR-GO 0.50%, and PU@SiR-GO 1.00%, besides the stretching vibration of the Si-O-Si and Si-C bands, the new occurrence of a band at 1612 cm^{-1} can be ascribed to the stretching vibration of the C=C band in GO molecules. The above measurements indicate that the SiR-GO coating has been deposited on the surface of PU foam through our dip-coating technology.

3.2 Mechanical properties

To further evaluate the effect of SiR-GO coating on the stress properties of PU foam composites, the mechanical properties of PU foam and PU foam composites were characterized by an in-plane cycle compression test. The compression stress-strain curves of the samples, at 10 cyclic times, are plotted in Figs. 2(a–e). With reference to the curve of the pristine PU in Fig. 2(a), the compression

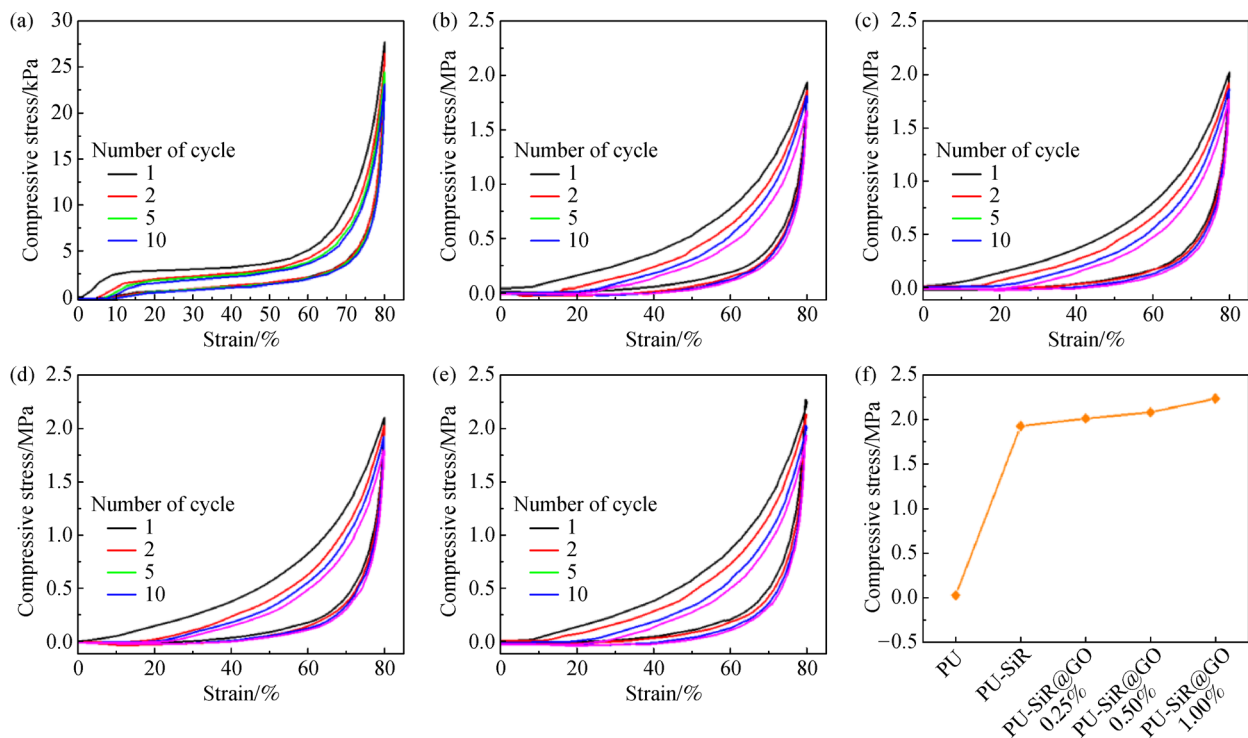


Fig. 2 The compressive stress-strain curves of (a) pristine PU, (b) PU@SiR, (c) PU@SiR-GO 0.25%, (d) PU@SiR-GO 0.50%, and (e) PU@SiR-GO 1.00% during ten loading-unloading cycles of compressive stress at 80% strain; (f) the maximum compressive stress of pristine PU and PU composites.

stress increases slowly when loading the applied stress, then exhibits a plateau, followed by rapidly increasing stress. After unloading the stress, the PU foam exhibits good compressibility with full recovery owing to its high porosity and elasticity [48]. The photographs recording the PU foam status under a compressing and releasing cycle are shown in Fig. S2(a) (cf. ESM). The PU foam itself is a deformable material under compression with excellent elasticity, which allows it to recover to its original state without compressive stress loss, even under 10 cyclic compressive tests. The compression stress-strain curves of PU@SiR, PU@SiR-GO 0.25%, PU@SiR-GO 0.50%, and PU@SiR-GO 1.00% at cyclic 10 times are shown in Figs. 2(b–e).

The PU composite compression stress increases when the applied stress is increased, and the plateau is not observed until the compressive stress is at 80% strain. As shown in Figs. S2(b–e), the remarkable phenomenon observed is that PU composites can recover to their original shape without any distinct plastic deformation after unloading stress. This can be associated with the deformable nature of SiR and GO, which could allow PU composites not to undergo plastic deformation when compressed by a certain external force at 80% compression strain. Therefore, the PU composites will not undergo plastic deformation during the compression process, which is verified in the cyclic compression testing of PU composites shown in Figs. 2(b–e). It needs to be noted that the maximum compression stress slightly decreases during the ten loading-unloading cycles. This may be associated with the compression of the SiR coating or SiR-GO coatings, causing micro-cracks to emerge and spread on the surface of PU composites during the compression process. Correspondingly, the micro-cracks would exert a negative influence on the mechanical performance of PU composites. This is consistent with reported work wherein the compressive stress of SiR coated PU foam showed a slight decrease, by 5%–10%, after the compression test [32].

A comparison of the maximum compressive stress of PU and PU composites is plotted in Fig. 2(f). It can be observed that the maximum compressive stress of PU@SiR, PU@SiR-GO 0.25%, PU@SiR-GO 0.50%, and PU@SiR-GO 1.00% are 1.93, 2.01, 2.08, and 2.24 MPa, respectively. All PU composites exhibit much higher compressive stress than that of pristine PU foam (27.7 kPa). This indicates that the deposition of SiR or SiR-GO coating can greatly improve the mechanical properties of PU composites. Notably, compared with PU@SiR, the compressive stress of PU@SiR-GO further increases with the incorporation of GO. The SiR contains a large amount of phenyl group, which is well known for its affinity with graphene sheets by π - π interaction. When SiR is mixed with GO sheets, it could be readily intercalated into the layer spacing of the sheets. Moreover, the high shear force during the stir process can produce the formation of π - π stacking and thus significantly enhanced the sheet/matrix interaction. Additionally, the GO nano-sheet itself has excellent mechanical properties; thus, the compressive stress exhibits a steady increase with increasing GO content. This is consistent with reported work in which the presence of GO can greatly improve the mechanical properties of composites [49]. In summary, the mechanical properties of PU foam composites are enhanced through coating with SiR on the skeleton surface without significantly reducing the elasticity.

3.3 Thermal stability

To evaluate the impact of incorporating GO into SiR, TGA was performed to investigate the effect of SiR-GO coating on the thermal properties of PU foam composites under N_2 atmosphere. The TGA and derivative thermogravimetric analysis (DTG) curves of PU and PU foam composites are shown in Figs. 3(a) and 3(b), respectively. For pristine PU foam, two thermal degradation steps were observed from the TGA and DTG curves. The first stage shows approximately 24.94% mass loss in the temperature

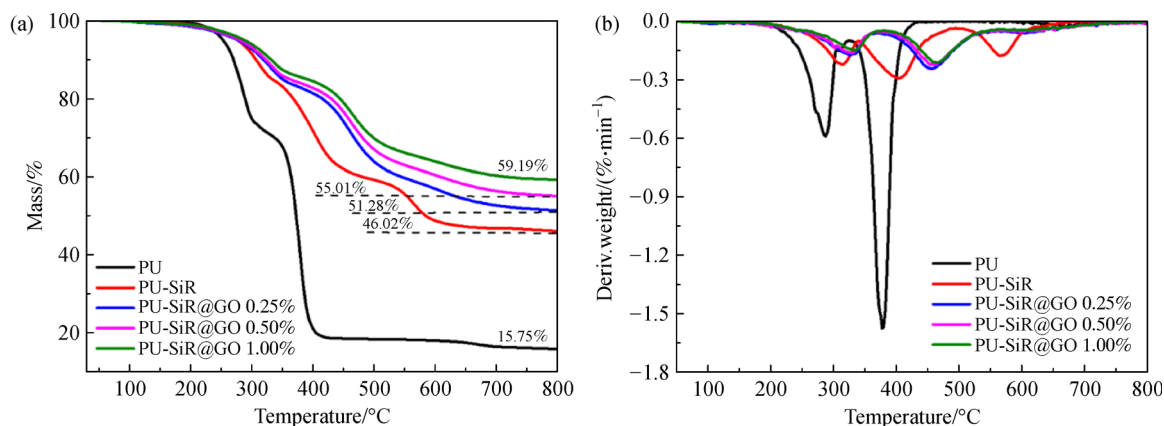


Fig. 3 (a) TGA and (b) DTG curves of pristine PU foam and PU foam composites.

range of 180 °C–300 °C (peak maximum at 288 °C), which can be ascribed to the liberation of diisocyanatos from the depolymerization of urethane and the disubstitution of urea groups. The second stage can be attributed to the decomposition of the remaining polyether chain [50], which shows approximately 49.04% mass loss in the temperature range of 350 °C–440 °C (peak maximum at 378 °C).

After coating the SiR, the PU@SiR composites exhibited three-stage decomposition behavior. The first degradation stage occurred between 215 °C and 345 °C, the temperature at the maximum weight loss rate was 314 °C and the weight loss was 14.91%. The thermal weight loss can be attributed to the production of water, which was generated from the condensation reaction of Si–OH groups [51]. The second stage of thermal degradation occurred between 345 °C and 495 °C, the temperature at the maximum weight loss rate was 400 °C and the weight loss was 24.27%. The weight loss can be ascribed to cyclic oligomer materials and cage-like small molecules derived from the “trickle” degradation of Si–OH groups. The third stage of thermal degradation occurred between 525 °C and 615 °C, the temperature at the maximum weight loss rate was 568 °C and the weight loss was 9.88%, which can be considered the weight loss caused by the breakage of Si–CH₃, Si–Ph, and other small molecules [52]. The detailed data including initial decomposition temperature ($T_{5\%}$), the maximum decomposition rate (R_{\max}), the temperature at maximum decomposition rate (T_{\max}), and the residue mass percent after heating to 800 °C are summarized in Table 1.

Compared with the TGA curve of PU, the $T_{5\%}$ of PU@SiR (272 °C) presents a rightward shift of approximately 19 °C compared to PU (253 °C). The R_{\max} of PU@SiR foam decreases from an R_{\max} of -1.575 to $-0.293\% \cdot \text{min}^{-1}$ and the T_{\max} of PU@SiR (405 °C) increased by 27 °C compared to the pristine PU (378 °C). Furthermore, the residue mass of PU@SiR after TGA is 46.02%, which is much higher than that of pristine PU (15.75%). Moreover, after incorporation of GO, all PU@SiR-GO composites exhibit similar three-stage decomposition behavior with PU@SiR. The $T_{5\%}$ of PU@SiR-GO 0.25%, PU@SiR-GO 0.50%, and PU@SiR-GO 1.00% presented a rightward shift of 23 °C, 27 °C and 34 °C, respectively, compared to PU (253 °C). The R_{\max} of PU@SiR-GO composites begins to decrease sharply after

coating with the SiR-GO layer. R_{\max} further decreases with increasing GO content and finally reaches a minimum rate at $-0.213\% \cdot \text{min}^{-1}$ for PU@SiR-GO 1.00%. Correspondingly, the T_{\max} of PU foam composites increased by 51 °C, 57 °C, and 62 °C compared to PU@SiR (405 °C), respectively. Furthermore, the residue mass of PU@SiR-GO 0.25%, PU@SiR-GO 0.50%, and PU@SiR-GO 1.00% after TGA are 51.28%, 55.01%, and 59.19%, respectively, which is much higher than that of PU@SiR (46.02%).

The abovementioned results indicate that incorporation of GO into SiR-GO coating can further enhance the thermal stability of PU foam, and the SiR-GO coated PU foam composites exhibit increased stable thermal stability with increasing GO content. The reason for this increased stability can be explained by the fact that GO contains polar OH and COOH groups, and GO backbones consist of polar Si–O units. The GO easily absorbs the polar Si–O bond, resulting in the formation of physical cross-linking points, which would increase the rigidity of siloxane chains and thus hinder the degradation of siloxane chains [53]. Additionally, GO can form a GO-SiR network in the SiR matrix, which acts as a barrier to inhibit the emission of volatile degradation products [54]. Therefore, the presence of the SiR-GO coating showed a synergistic effect on improving the thermal stability of PU foam composites.

3.4 Flame retardancy

The incorporation of a SiR-GO hybrid coating can significantly enhance the thermal stability of PU composites. To better understand its role and how SiR-GO coating can protect the PU foam, the combustion behavior of PU and PU foam composites were investigated by a vertical combustion test. The combustion process of the composites is shown in Fig. 4. As shown in Fig. 4(a), when the pristine PU foam is ignited by an alcohol burner within 1 s, then removed; the flame quickly spreads to the entire sample, yielding a large amount of smoke and dripping molten mass. The sample is completely combusted within 3 s (see Movie S1 in ESM). Comparatively, in Fig. 4(b), the PU@SiR sample is exposed to the fire source for 5 s, and the flame spreads to the entire sample, accompanied by a large amount of smoke but without molten dripping mass (see Movie S2 in ESM). The PU@SiR sample is

Table 1 The detailed data of PU and PU composites

Specimen	$T_{5\%}/^{\circ}\text{C}$	$R_{\max}/(\% \cdot \text{min}^{-1})$	$T_{\max}/^{\circ}\text{C}$	Residue/%
PU	253	-1.575	378	15.75
PU@SiR	272	-0.293	405	46.02
PU@SiR-GO 0.25%	276	-0.243	456	51.28
PU@SiR-GO 0.50%	280	-0.224	462	55.01
PU@SiR-GO 1.00%	287	-0.213	467	59.19

completely combusted with the combustion time extending to 31 s, indicating that the SiR coating has a positive effect in reducing the flammability of the PU foam. Figure 4(c) shows the combustion process of PU@SiR-GO 0.25% when it is exposed to the fire source for 5 s. A phenomenon similar to the PU@SiR sample occurs for PU@SiR-GO 0.25%. Still, the combustion time is prolonged to 40 s (see Movie S3 in ESM), which indicates that incorporating GO into SiR can improve the fire resistance of PU foam composites.

To verify the role that GO plays in improving flame retardancy, the combustion process of PU@SiR-GO 0.50% and PU@SiR-GO 1.00% were monitored. The digital photos in Fig. 4(d) show that PU@SiR-GO 0.50% is on fire for 5 s and then the fire source is removed. Although the fire still spread quickly to the entire sample, the combustion trend becomes weak after the sample leaves the fire source and is self-extinguished after 11 s (see Movie S4 in ESM). After careful observation, white

ash appears to have been generated on the composite surface. A similar phenomenon was also observed in the combustion process of PU@SiR-GO 1.00%. As shown in Fig. 4(e), after the PU@SiR-GO sample was removed from the fire source after exposure to fire for 5 s, the sample self-extinguished within 5 s (see Movie S5 in ESM). It is noted that, the self-extinguishing time is 6 s shorter than that of PU@SiR-GO 0.50%, indicating that the flame retardancy of the PU composite increases with increasing GO content.

To further evaluate the flame retardancy of PU composites, cone calorimetry tests were carried out to provide comprehensive insight into the fire risks via a series of parameters such as HRR, total heat release (THR), total smoke release (TSR), mass loss rate (MLR), and char content. The results are shown in Fig. 5.

As shown in Fig. 5(a), the peak HRR of PU is $223 \text{ kW}\cdot\text{m}^{-2}$. After coating with SiR or SiR-GO, the HRR values of PU@SiR, PU@SiR-GO 0.25%, PU@SiR-GO 0.50%, and PU@SiR-GO 1.00% drastically decreased

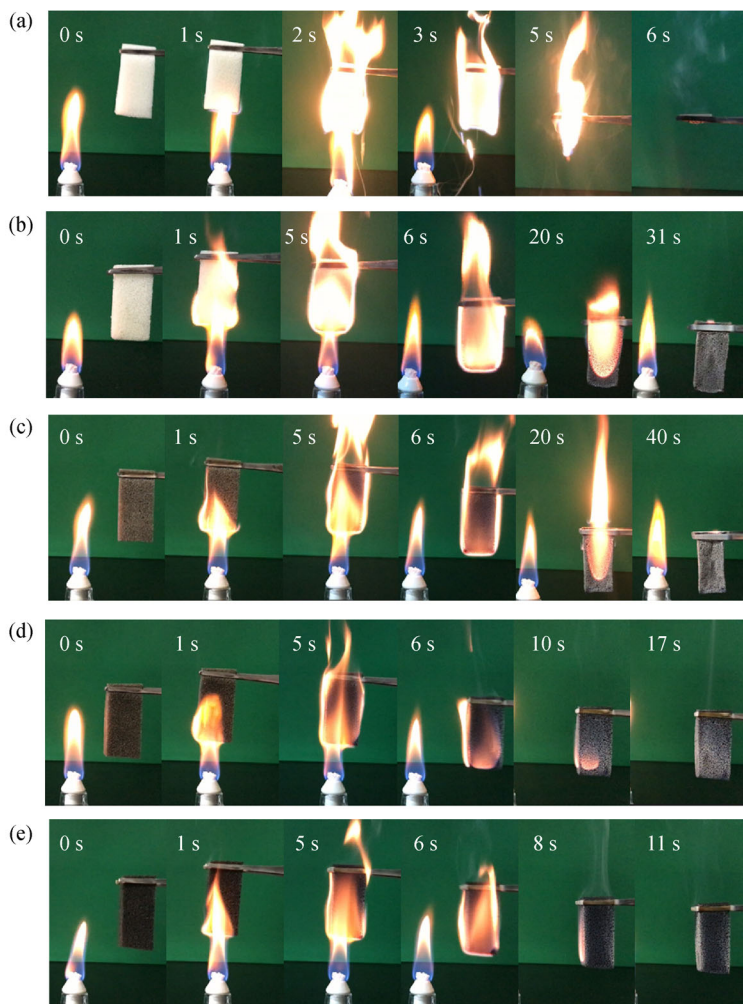


Fig. 4 Vertical combustion tests of (a) pristine PU, (b) PU@SiR, (c) PU@SiR-GO 0.25%, (d) PU@SiR-GO 0.50%, and (e) PU@SiR-GO 1.00%.

by 50.0%, 61.2%, 64.2%, and 65.8%, respectively, compared with that of the PU foam. PU burned completely in 67 s, and PU@SiR burned completely in 100 s, indicating that the PU@SiR has improved anti-combustion performance. PU@SiR-GO 0.25%, PU@SiR-GO 0.50%, and PU@SiR-GO 1.00% completed combustion in 120, 133, and 140 s, respectively. The longer burning time, compared to PU@SiR, shows that graphene can improve the flame retardancy of PU composites. With reference to the THR curves shown in Fig. 5(b), the THR curve of PU@SiR presents a higher value than that of PU. This could be attributed to the intrinsic flammability of the SiR coating due to a plentiful number of combustible groups like methyl and phenyl.

The mass of coated SiR is two times that of PU foam, thus the PU@SiR released heat at a rate during combustion. We have previously reported a similar phenomenon [32]. With reference to the THR curves of PU@SiR-GO composites, the THR values of PU@SiR-GO 0.25%, PU@SiR-GO 0.50%, and PU@SiR-GO 1.00% are lower compared with that of PU@SiR, indicating the incorporation of GO into SiR can decrease the THR values of the composite. Furthermore, The THR values present a further decrease with increasing GO content. The THR

value of PU@SiR-GO 1.00% decreases to a minimum of $6.2 \text{ MJ} \cdot \text{m}^{-2}$. Meanwhile, the TSR curves of PU and PU composites in Fig. 5(c) display similar THR curve results. The TSR of PU@SiR is the highest among all samples, even larger than pristine PU. After incorporating GO into SiR, the TSR curves of PU@SiR-GO 0.25%, PU@SiR-GO 0.50%, and PU@SiR-GO 1.00% start to decrease. However, for PU composites with low GO content, like PU@SiR-GO 0.25% and PU@SiR-GO 0.50%, the TSR values are still larger than that of PU. When the GO content climbs to 1.00%, PU@SiR-GO 1.00%, the lowest peak of TSR is present among the samples, indicating that smoke toxicity is reduced during the combustion process. This can be ascribed to the incorporation of graphene, which can provide a so-called “tortuous path” effect that significantly alters the diffusion path of pyrolysis products and promotes the formation of a compact, dense, and uniform char layer in condensed phase during the combustion of the polymer matrix. Furthermore, GO may absorb polycyclic aromatic hydrocarbon (PAH) species, and these active PAH species propagate on the graphene that serves as a template of micro-char. Eventually, PAH are converted to carbon on graphene [55]. Under the combination of these two actions, the

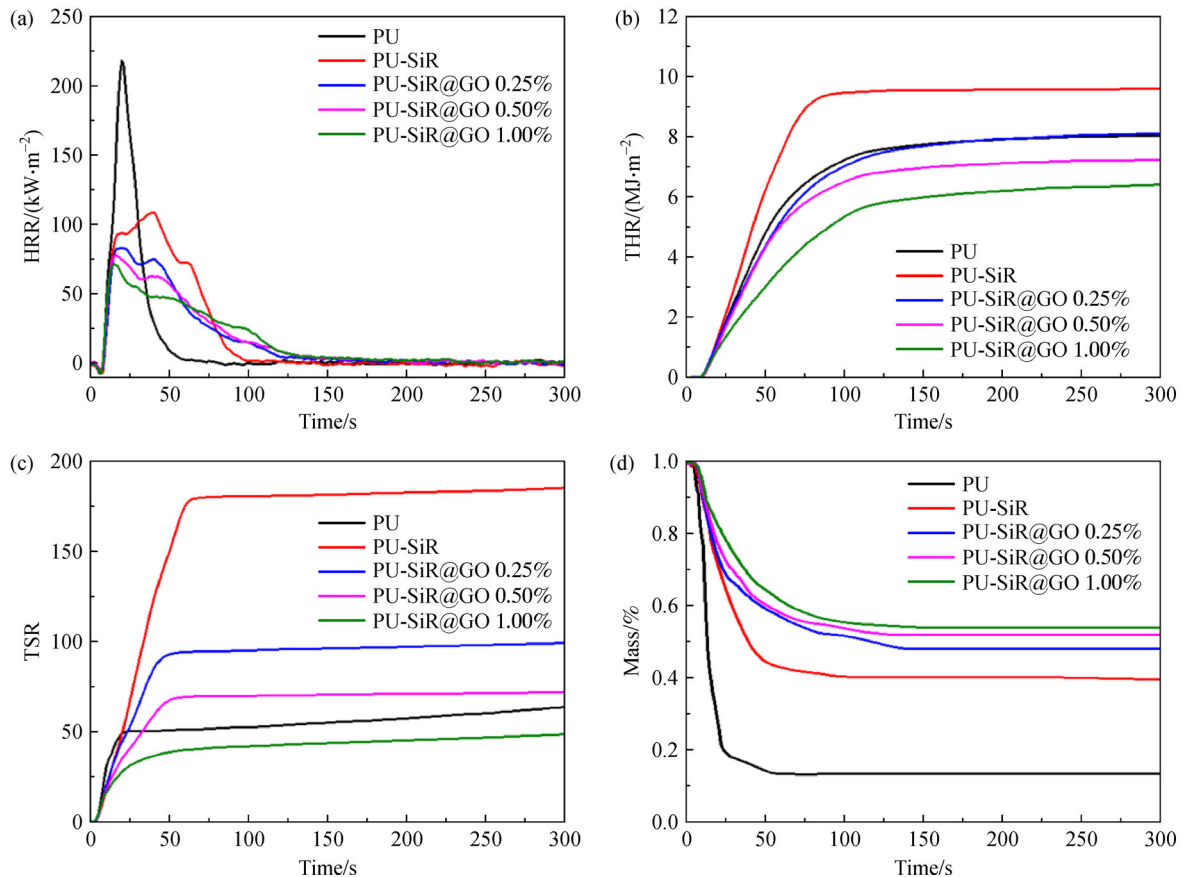


Fig. 5 (a) HRR, (b) THR, (c) TSR, and (d) mass loss curves of pristine PU foam and PU foam composites.

production of toxic smoke is reduced. As shown in MLR curves in Fig. 5(d), the residue mass of PU is nearly zero, indicating that no char is formed during PU combustion. After coating SiR or SiR-GO, the residue mass of PU@SiR, PU@SiR-GO 0.25%, PU@SiR-GO 0.50%, and PU@SiR-GO 1.00% PU composites increase to 34.9%, 47.9%, 51.7%, and 55.4% respectively. This is consistent with the results in Figs. 6(a–e), which show photographs of PU and PU composites after cone calorimetry tests. Figure 6(a) shows no remaining residue, implying that the PU foam combusted completely. Figure

6(b) shows that the residue of PU@SiR is hoary and deformed under fire attack. After the incorporation of GO, the residue of PU composites is markedly different than that of PU@SiR. As shown in Figs. 6(c–e), all the residues keep their initial shape. Apart from the residue of PU@SiR-GO 0.25% in Fig. 6(c), which is cracked though not severe, the residue of PU@SiR-GO 0.50% and PU@SiR-GO 1.00% can keep their integrated structure.

The results of LOI for all samples are summarized in Fig. 6(f). The LOI of PU foam increases from 14.6% to 24.8% after coating with SiR. After incorporating GO, the

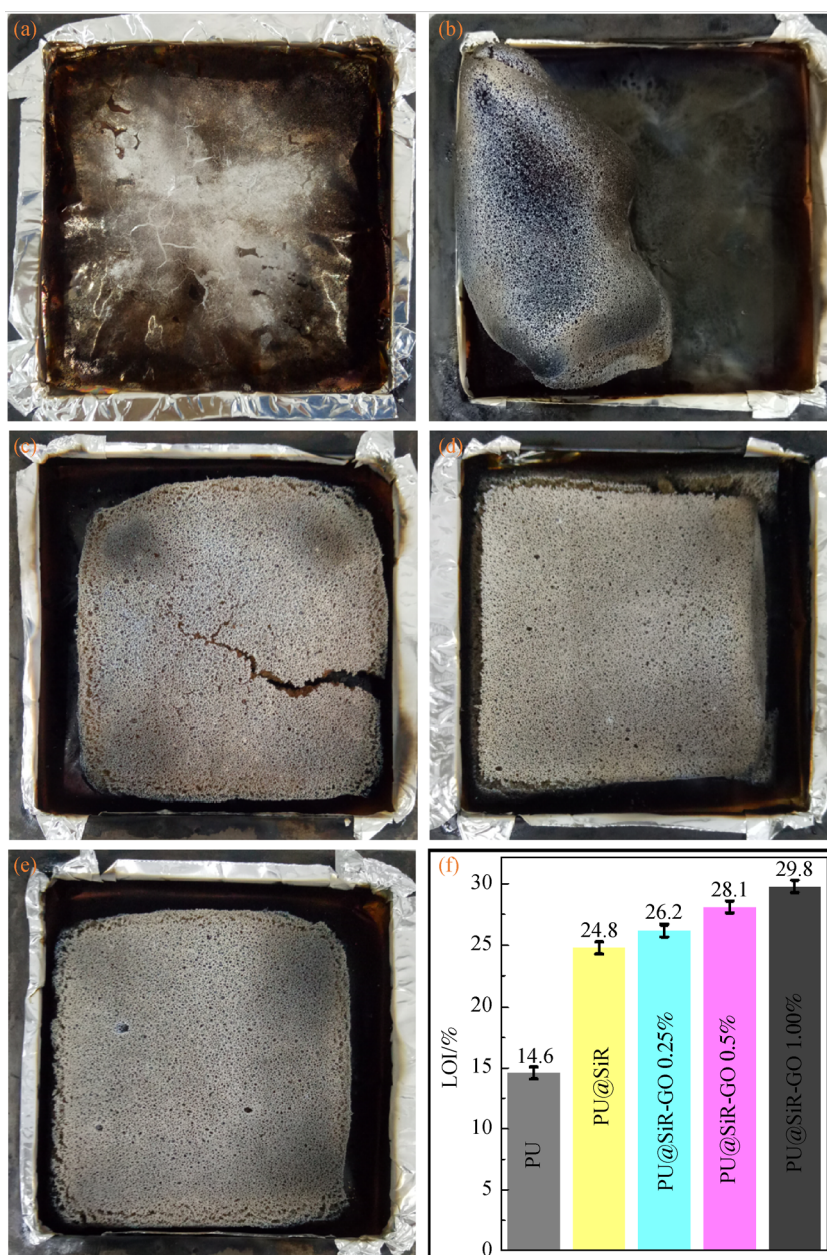


Fig. 6 Residues after conical calorimeter testing of (a) pristine PU, (b) PU@SiR, (c) PU@SiR-GO 0.25%, (d) PU@SiR-GO 0.50%, and (e) PU@SiR-GO 1.00%; (f) LOI of pristine PU and PU composites.

LOI of PU@SiR-GO 0.25%, PU@SiR-GO 0.50%, and PU@SiR-GO 1.00% composites further increase to 26.2%, 28.1%, and 29.8%, respectively. The PU composites gradually evolve to become difficult-to-combust material from easy-to-combust material. Our results confirm that the presence of SiR-GO coating can significantly enhance the flame retardancy of PU composites with increasing GO content.

3.5 Flame-retardant mechanism analysis

To reveal the flame-retardant mechanism of the hybrid SiR-GO coating, the residual char of PU@SiR-GO 1.00% composite was investigated. In particular, the outstanding flame retardancy of this sample during the combustion process was considered. The components inside and outside the skeleton surface were characterized by FTIR spectra, as shown in Fig. 7(a). The combusted PU@SiR-GO composites maintain their structural integrity (see Fig. 7(b)). After carefully cutting the PU@SiR-GO composites with a blade, the inside zone exhibits a good condition,

though appearing dark, which is likely due to the presence of GO nano-sheets. Although both the outside and inside zones keep the integrity and dark appearance, it is worthy to note that white powders are found outside the skeleton surface but not inside. To clarify the composition of this white powder, the white powder was carefully collected and characterized using FTIR and XRD. The red curve in Fig. 7(a) is the FTIR spectrum of the white powder. Two distinct peaks were observed: one peak at 1080 cm^{-1} corresponds to the stretch vibration of the Si–O–Si bond, and the other peak at 794 cm^{-1} corresponds to the stretch vibration of the Si–C bond. Meanwhile, the stretching vibration of the C–H band at 2980 and 2880 cm^{-1} is not detected, indicating the SiR has completely decomposed under thermal attack. The XRD curve obtained for the white powder is plotted in Fig. S3 (cf. ESM); a diffraction pattern peak at approximately $2\theta = 23^\circ\text{--}24^\circ$ was detected, which can be attributed to the diffraction peak of amorphous SiO_2 [56]. These results further confirmed that the white powder layer is mainly composed of nano-silica, which is likely formed during combustion. The

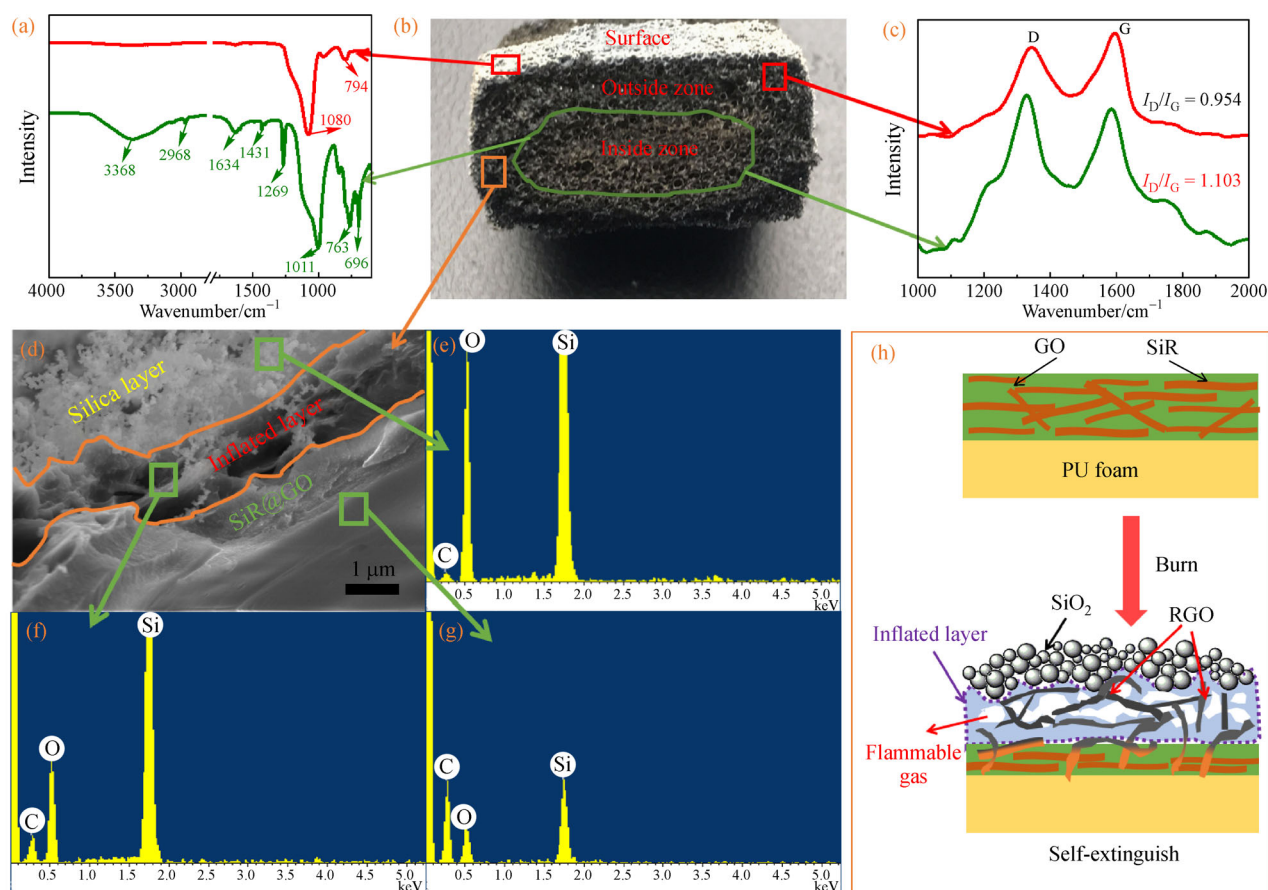


Fig. 7 (a) FTIR curves of PU-SiR-GO 1.00% after the combustion test at the outer and inner zones; (b) cross-sectional photo of PU-SiR-GO 1.00% after the combustion test; (c) Raman curves of PU@SiR-GO 1.00% after the combustion test at the outer and inner zones. SEM image of PU@SiR-GO 1.00% at (d) the sectional edge and with EDS after the combustion test at the (e) silica layer, (f) inflated layer, and (g) SiR-GO layer. (h) Schematic illustration of the combustion process of PU@SiR-GO 1.00%.

green curve in Fig. 7(a) reflects the inner zone of PU@SiR-GO 1.00% after combustion. The bonds at 3368, 2968, 1011, and 1269 cm^{-1} are assigned to the stretch vibration of N–H, C–H, Si–O–Si, and C=C bonds, respectively. The peak at 1431 cm^{-1} is the vibration of the aromatic ring, and 1269 cm^{-1} conforms to the symmetric deformation vibration of Si–CH₃. The bands at 763 cm^{-1} and 696 cm^{-1} are in accordance with C–H planar swing vibration and Si–C stretch vibration, respectively. The presence of N–H and Si–CH₃ indicates that the inner zone does not show an evident thermal degradation of SiR and PU, where the structural integrity and composition are preserved well.

To clarify whether GO has a chemical reaction during combustion, Raman spectroscopy was carried out on the outside and inside regions of the PU composites (see Fig. 7(b)) after combustion. The results are shown in Fig. 7(c), where the red and green curves correspond to the outside and inside of the PU composites, respectively. The two characteristic bands at 1340 cm^{-1} and 1560 cm^{-1} correspond to the characteristic D and G peaks, respectively. From the Raman spectra, the intensity ratio values of the D and G peaks (I_D/I_G) are calculated as 0.954 and 1.103 for the inside and outside regions, respectively. This shows a side defect in the graphene structure [57]. Compared to the I_D/I_G value of the inside region of the PU composites, the I_D/I_G value of the outside region decreased, implying the reduction of GO into reduced GO (RGO) [58] and transformation of GO into char [59]. Furthermore, after cutting the PU@SiR-GO 1.00% composites after combustion, SEM was conducted to observe the morphologies of residual char at the sectional edge. As shown in Fig. 7(d), three distinct layers are present. The outside layer is a porous nano-silica and char layer, which was discussed earlier according to the FTIR and XRD results. The sandwich-like layer is a porous inflated layer, which is mainly composed of porous nano-silica, not-fully decomposed SiR, GO, and thermally reduced RGO. This layer plays the role of a buffer zone that inhibits flammable and volatile organic compounds, which support combustion, from being transported to the surface. The layer also can suppress the diffusion of oxygen from outside to inside the PU composite.

The inside layer is an undecomposed SiR-GO layer, and the high-magnification SEM image of the outside region clearly reflects the presence of the three layers in Fig. S4 (cf. ESM). Furthermore, the SEM-EDS results for the three

layers are shown in Figs. 7(e–g) and the detailed contents of Si, C, and O elements are summarized in Table 2. From the inner SiR-GO layer to the sandwich-like inflated layer and outside the silica layer, the content of Si and O increases, whereas the C content decreases.

Based on the compositional characterization of the three layers, including the Si, O, and C content from inside to outside regions, the possible formation mechanism of a protective barrier layer and the flame-retardant mechanism for PU@SiR-GO composites can be speculated (see Fig. 7(h)). Once the SiR-GO coated PU encounters fire, the SiR-GO coating is transformed into a compact hybrid-silica char protective layer in the outside zone. During the combustion process, the organic components in SiR decompose, and compact nano-silica is produced. As the combustion proceeds, the GO is thermally reduced into RGO [58] and transformed into char [59]. This is confirmed from the decrease of I_D/I_G in Fig. 7(c) and the detection of C in Fig. 7(e).

Considering the GO content is 1.00% of the initial SiR weight, it is reasonable to assume that Si and O are the dominant elements in the outside region of the PU composites. The porous nano-silica and RGO char produced as a protective layer can synergistically suppress the transportation of heat and oxygen. Undoubtedly, the porous nano-silica and RGO char layer are not compact enough to completely inhibit the heat transfer and combustible gas diffusion due to the porous structure. The thermal degradation of SiR would not terminate, but the degradation rate would slow down due to the presence of the barrier. Therefore, the inflated layer in the sandwich, which is mainly composed of porous nano-silica, would form not-fully-decomposed SiR, GO, and thermally reduced RGO char. The inner layer is the initial SiR-GO coating, which can be confirmed by the inner structural integrity and composition analysis comparison (see Figs. 7(f–g)). Furthermore, no white powder is detected, implying SiR did not decompose into silica. Therefore, under the combined effects of nano-silica and RGO char in the outer layer, and the physical barrier of the inflated layer, heat and oxygen transport from outside of the foam is inhibited, and the supply of combustible degradation products is suppressed to avoid further combustion. Therefore, the inside layer of PU@SiR-GO is well protected, and the PU@SiR-GO composites exhibit excellent flame retardancy.

Table 2 Elemental analysis of PU@SiR-GO 1.00% at outside, inflated, and inside layer regions before and after the combustion test

PU@Si-GO 1.00%	C/%		O/%		Si/%	
	wt	atom	wt	atom	wt	atom
Outside layer after combustion	3.32	5.43	56.92	63.93	39.76	30.64
Inflated layer after combustion	29.14	28.44	47.29	56.92	32.19	24.27
Inside layer after combustion	47.31	53.08	27.55	26.27	25.14	20.65
Outside layer before combustion	47.65	53.26	28.06	26.35	25.29	21.45

4 Conclusions

In this article, we developed a facile and effective strategy to fabricate highly flame-retardant and flexible PU foam composites. The approach first involves the incorporation of GO nano-sheets into a SiR solution, then dipping the PU foam into the SiR-GO solution, removing and curing. Our results show the SiR-GO coating improves the thermal and mechanical stability of the PU foam composites, exerting a synergistic effect on the enhancement of the flame retardancy with increasing GO content. When the GO content was 0%, 0.25%, 0.50%, and 1.00%, the HRR of the PU composites significantly decreased by 50.02%, 61.18%, 64.19%, and 65.84%, respectively, and the LOI increased from the pristine foam value of 14.6% to 24.8%, 26.2%, 28.1%, and 29.8%, respectively. SEM analysis showed that three layers are formed after the samples self-extinguish. The outer layer is a porous nano-silica and char layer that effectively suppresses heat transport and oxygen diffusion. The sandwich-like layer is an inflated porous layer that can accommodate flammable, volatile organic compounds, and act as a buffer zone to inhibit the transport of these compounds. This layer also suppresses the diffusion of oxygen from outside of the PU composites. Therefore, the inside SiR-GO layer is well preserved without thermal decomposition. This study demonstrates, for the first-time, that incorporating GO into SiR can generate porous nano-silica/char and inflated layers during the combustion process, which suppresses heat transport and diffusion of flammable, volatile organic compounds, resulting in PU@SiR-GO composites with excellent flame retardancy.

Acknowledgements This work was supported by the National Key Research and Development Program (Grant No. 2017YFB0307700), and the Department of Scientific and Technology of Zhejiang Province (LGG18E030007, LGG19E030007), and the Project for the Innovation of High Level Returned Overseas Scholars (or team) in Hangzhou. We also acknowledge the support from Collaborative Innovation Center of Zhejiang Province for the Manufacture of Fluorine and Silicone Fine Chemicals and Materials (FSi2018A028, FSi2018B004), and professional development project for domestic visiting scholars in universities (FX2017054).

Electronic Supplementary Material Supplementary material is available in the online version of this article at <https://doi.org/10.1007/s11705-020-1988-8> and is accessible for authorized users.

References

1. Lefebvre J, Bastin B, Le Bras M, Duquesne S, Paleja R, Delobel R. Thermal stability and fire properties of conventional flexible polyurethane foam formulations. *Polymer Degradation & Stability*, 2005, 88(1): 28–34
2. Song K, Zhang Y, Meng J, Green E C, Tajaddod N, Li H, Minus M L. Structural polymer-based carbon nanotube composite fibers: understanding the processing-structure-performance relationship. *Materials (Basel)*, 2013, 6(6): 2543–2577
3. Zia K M, Bhatti H N, Ahmad Bhatti I. Methods for polyurethane and polyurethane composites, recycling and recovery: a review. *Reactive & Functional Polymers*, 2007, 67(8): 675–692
4. Tian H, Yao Y, Zhang S, Wang Y, Xiang A. Enhanced thermal stability and flame resistance of rigid polyurethane-imide foams by varying copolymer composition. *Polymer Testing*, 2018, 67: 68–74
5. Haile M, Fomete S, Lopez I D, Grunlan J C. Aluminum hydroxide multilayer assembly capable of extinguishing flame on polyurethane foam. *Journal of Materials Science*, 2016, 51(1): 375–381
6. Denecker C, Liggat J, Snape C. Relationship between the thermal degradation chemistry and flammability of commercial flexible polyurethane foams. *Journal of Applied Polymer Science*, 2006, 100(4): 3024–3033
7. Wang C Q, Ge F Y, Sun J, Cai Z S. Effects of expandable graphite and dimethyl methylphosphonate on mechanical, thermal, and flame-retardant properties of flexible polyurethane foams. *Journal of Applied Polymer Science*, 2013, 130(2): 916–926
8. Bourbigot S, Duquesne S. Fire retardant polymers: recent developments and opportunities. *Journal of Materials Chemistry*, 2007, 17(22): 2283–2300
9. Cain A A, Nolen C R, Li Y C, Davis R, Grunlan J C. Phosphorous-filled nanobrick wall multilayer thin film eliminates polyurethane melt dripping and reduces heat release associated with fire. *Polymer Degradation & Stability*, 2013, 98(12): 2645–2652
10. Zhang M, Zhang J, Chen S, Zhou Y, Luo Z. Effects of a novel phosphorus-nitrogen flame retardant on rosin-based rigid polyurethane foams. *Polymer Degradation & Stability*, 2015, 120: 427–434
11. Yang R, Hu W, Xu L, Song Y, Li J. Synthesis, mechanical properties and fire behaviors of rigid polyurethane foam with a reactive flame retardant containing phosphazene and phosphate. *Polymer Degradation & Stability*, 2015, 122: 102–109
12. Zhang L, Wang F, Zhang X, Zou J J. Synthesis of aluminum nanoparticles as additive to enhance ignition and combustion of high energy density fuels. *Frontiers of Chemical Science and Engineering*, 2018, 12(3): 358–366
13. Yang H, Wang X, Song L, Yu B, Yuan Y, Hu Y, Yuen R K K. Aluminum hypophosphite in combination with expandable graphite as a novel flame retardant system for rigid polyurethane foams. *Polymers for Advanced Technologies*, 2014, 25(9): 1034–1043
14. Wang X, Zhang P, Huang Z, Xing W, Song L, Hu Y. Effect of aluminum diethylphosphinate on the thermal stability and flame retardancy of flexible polyurethane foams. *Fire Safety Journal*, 2019, 106: 72–79
15. Bourbigot S, Bras M L, Leeuwendal R, Shen K K, Schubert D. Recent advances in the use of zinc borates in flame retardancy of EVA. *Polymer Degradation & Stability*, 1999, 64(3): 419–425
16. Gao Y, Wu J, Wang Q, Wilkie C, O'Hare D. Flame retardant polymer/layered double hydroxide nanocomposites. *Journal of Materials Chemistry. A, Materials for Energy and Sustainability*, 2014, 2(29): 10996–11016
17. Wu Q, Gong L, Li Y, Cao C, Tang L, Wu L, Zhao L, Zhang G, Li S, Gao J, Li Y, Mai Y W. Efficient flame detection and early warning sensors on combustible materials using hierarchical graphene oxide/silicone coatings. *ACS Nano*, 2018, 12(1): 416–424
18. Liu C, Fang Y, Miao X, Pei Y, Yan Y, Xiao W, Wu L. Facile

- fabrication of superhydrophobic polyurethane sponge towards oil-water separation with exceptional flame-retardant performance. *Separation and Purification Technology*, 2019, 229: 115801
19. Li Y, Kim Y S, Shields J, Davis R. Controlling polyurethane foam flammability and mechanical behaviour by tailoring the composition of clay-based multilayer nanocoatings. *Journal of Materials Chemistry. A, Materials for Energy and Sustainability*, 2013, 1 (41): 12987–12997
 20. Wang W, Pan Y, Pan H, Yang W, Liew K M, Song L, Hu Y. Synthesis and characterization of MnO₂ nanosheets based multilayer coating and applications as a flame retardant for flexible polyurethane foam. *Composites Science and Technology*, 2016, 123: 212–221
 21. Pan H, Shen Q, Zhang Z, Yu B, Lu Y. MoS₂-filled coating on flexible polyurethane foam via layer-by-layer assembly technique: flame-retardant and smoke suppression properties. *Journal of Materials Science*, 2018, 53(12): 9340–9349
 22. Cain A A, Plummer M G B, Murray S E, Bolling L, Regev O, Grunlan J C. Iron-containing, high aspect ratio clay as nanoarmor that imparts substantial thermal/flame protection to polyurethane with a single electrostatically-deposited bilayer. *Journal of Materials Chemistry. A, Materials for Energy and Sustainability*, 2014, 2(41): 17609–17617
 23. Kim Y S, Harris R, Davis R. Innovative approach to rapid growth of highly clay-filled coatings on porous polyurethane foam. *ACS Macro Letters*, 2012, 1(7): 820–824
 24. Cho J H, Vasagar V, Shanmuganathan K, Jones A R, Nazarenko S, Ellison C J. Bioinspired catecholic flame retardant nanocoating for flexible polyurethane foams. *Chemistry of Materials*, 2015, 27(19): 6784–6790
 25. Laufer G, Kirkland C B, Morgan A, Grunlan J. Exceptionally flame retardant sulfur-based multilayer nanocoating for polyurethane prepared from aqueous polyelectrolyte solutions. *ACS Macro Letters*, 2013, 2(5): 361–365
 26. Mu X, Yuan B, Pan Y, Feng X, Duan L, Zong R, Hu Y. A single α -cobalt hydroxide/sodium alginate bilayer layer-by-layer assembly for conferring flame retardancy to flexible polyurethane foams. *Materials Chemistry and Physics*, 2017, 191: 52–61
 27. Pan Y, Liu L, Cai W, Hu Y, Jiang S, Zhao H. Effect of layer-by-layer self-assembled sepiolite-based nanocoating on flame retardant and smoke suppressant properties of flexible polyurethane foam. *Applied Clay Science*, 2019, 168: 230–236
 28. Wang W, Pan H, Yu B, Pan Y, Song L, Liew K M, Hu Y. Fabrication of carbon black coated flexible polyurethane foam for significantly improved fire safety. *RSC Advances*, 2015, 5(69): 55870–55878
 29. Carosio F, Fina A. Three organic/inorganic nanolayers on flexible foam allow retaining superior flame retardancy performance upon mechanical compression cycles. *Frontiers in Materials*, 2019, 6: 20
 30. Holder K M, Cain A A, Plummer M G, Stevens B E, Odenborg P K, Morgan A B, Grunlan J C. Carbon nanotube multilayer nanocoatings prevent flame spread on flexible polyurethane foam. *Macromolecular Materials and Engineering*, 2016, 301(6): 665–673
 31. Zhang X, Shen Q, Zhang X, Pan H, Lu Y. Graphene oxide-filled multilayer coating to improve flame-retardant and smoke suppression properties of flexible polyurethane foam. *Journal of Materials Science*, 2016, 51(23): 10361–10374
 32. Wu Q, Zhang Q, Zhao L, Li S, Wu L, Jiang J, Tang L. A novel and facile strategy for highly flame retardant polymer foam composite materials: transforming silicone resin coating into silica self-extinguishing layer. *Journal of Hazardous Materials*, 2017, 336: 222–231
 33. Xie H, Yang W, Yuen A C Y, Xie C, Xie J, Lu H, Yeoh G H. Study on flame retarded flexible polyurethane foam/alumina aerogel composites with improved fire safety. *Chemical Engineering Journal*, 2017, 311: 310–317
 34. Kim Y S, Davis R, Cain A A, Grunlan J C. Development of layer-by-layer assembled carbon nanofiber-filled coatings to reduce polyurethane foam flammability. *Polymer*, 2011, 52(13): 2847–2855
 35. Chen P, Zhao Y, Wang W, Zhang T, Song S. Correlation of montmorillonite sheet thickness and flame retardant behavior of a chitosan-montmorillonite nanosheet membrane assembled on flexible polyurethane foam. *Polymers*, 2019, 11(2): 213
 36. Hai Y, Wang C, Jiang S, Liu X. Layer-by-layer assembly of aerogel and alginate toward self-extinguishing flexible polyurethane foam. *Industrial & Engineering Chemistry Research*, 2020, 59(1): 475–483
 37. Lin B, Yuen A C Y, Li A, Zhang Y, Chen T B Y, Yu B, Lee E W M, Peng S, Yang W, Lu H, Chan Q N, Yeoh G H, Wang C H. Mxene/chitosan nanocoating for flexible polyurethane foam towards remarkable fire hazards reductions. *Journal of Hazardous Materials*, 2020, 381: 120952
 38. Pan H, Pan Y, Wang W, Song L, Hu Y, Liew K M. Synergistic effect of layer-by-layer assembled thin films based on clay and carbon nanotubes to reduce the flammability of flexible polyurethane foam. *Industrial & Engineering Chemistry Research*, 2014, 53(37): 14315–14321
 39. Ji X, Xu Y, Zhang W, Cui L, Liu J. Review of functionalization, structure and properties of graphene/polymer composite fibers. *Composites. Part A, Applied Science and Manufacturing*, 2016, 87: 29–45
 40. Nine M J, Cole M A, Tran D N H, Losic D. Graphene: a multipurpose material for protective coatings. *Journal of Materials Chemistry. A, Materials for Energy and Sustainability*, 2015, 3(24): 12580–12602
 41. Maddalena L, Carosio F, Gomez J, Saracco G, Fina A. Layer-by-layer assembly of efficient flame retardant coatings based on high aspect ratio graphene oxide and chitosan capable of preventing ignition of PU foam. *Polymer Degradation & Stability*, 2018, 152: 1–9
 42. Li Y, Mannen S, Schulz J, Grunlan J C. Growth and fire protection behavior of POSS-based multilayer thin films. *Journal of Materials Chemistry*, 2011, 21(9): 3060–3069
 43. Yang Z, Han S, Zhang R, Feng S, Zhang C, Zhang S. Effects of silphenylene units on the thermal stability of silicone resins. *Polymer Degradation & Stability*, 2011, 96(12): 2145–2151
 44. Zhou W, Yang H, Guo X, Lu J. Thermal degradation behaviors of some branched and linear polysiloxanes. *Polymer Degradation & Stability*, 2006, 91(7): 1471–1475
 45. Hamdani S, Longuet C, Perrin D, Lopez-cuesta J, Ganachaud F. Flame retardancy of silicone-based materials. *Polymer Degradation*

- & Stability, 2009, 94(4): 465–495
46. Jia P, Liu H, Liu Q, Cai X. Thermal degradation mechanism and flame retardancy of MQ silicone/epoxy resin composites. *Polymer Degradation & Stability*, 2016, 134: 144–150
 47. Hummers W S Jr, Offeman R E. Preparation of graphitic oxide. *Journal of the American Chemical Society*, 1958, 80(6): 1339–1339
 48. Davis R, Li Y, Kim Y S R, Shields J. Controlling foam flammability and mechanical behavior by tailoring the composition of clay-based multilayer nanocoatings. *Advanced Functional Materials*, 2013, 41 (1): 12987–12997
 49. Wan Y, Tang L, Gong L, Yan D, Li Y, Wu L, Jiang J, Lai G. Grafting of epoxy chains onto graphene oxide for epoxy composites with improved mechanical and thermal properties. *Carbon*, 2014, 69 (2): 467–480
 50. Pan H, Yu B, Wang W, Pan Y, Song L, Hu Y. Comparative study of layer by layer assembled multilayer films based on graphene oxide and reduced graphene oxide on flexible polyurethane foam: flame retardant and smoke suppression properties. *RSC Advances*, 2016, 6 (115): 114304–114312
 51. Patel M, Swain A C. Thermal stability of poly(*m*-carborane-siloxane) elastomers. *Polymer Degradation & Stability*, 2004, 83(3): 539–545
 52. Jovanovic J D, Govedarica M N, Dvornic P R, Popovic I G. The thermogravimetric analysis of some polysiloxanes. *Polymer Degradation & Stability*, 1998, 61(1): 87–93
 53. Wang X, Dou W. Preparation of graphite oxide (GO) and the thermal stability of silicone rubber/GO nanocomposites. *Thermo-chimica Acta*, 2012, 529: 25–28
 54. Ma W, Li J, Zhao X. Improving the thermal and mechanical properties of silicone polymer by incorporating functionalized graphene oxide. *Journal of Materials Science*, 2013, 48(15): 5287–5294
 55. Wang X, Kalali E N, Wan J, Wang D. Carbon-family materials for flame retardant polymeric materials. *Progress in Polymer Science*, 2017, 69: 22–46
 56. Deng Y, Qi D, Deng C, Zhang X, Zhao D. Superparamagnetic high-magnetization microspheres with an Fe₃O₄@SiO₂ core and perpendicularly aligned mesoporous SiO₂ shell for removal of microcystins. *Journal of the American Chemical Society*, 2008, 130 (1): 28–29
 57. Gong L X, Pei Y B, Han Q Y, Zhao L, Wu L B, Jiang J X, Tang L C. Polymer grafted reduced graphene oxide sheets for improving stress transfer in polymer composites. *Composites Science and Technology*, 2016, 134: 144–152
 58. Shi Y, Li L J. Chemically modified graphene: flame retardant or fuel for combustion? *Journal of Materials Chemistry*, 2011, 21(10): 3277–3279
 59. Higginbotham A L, Lomeda J R, Morgan A B, Tour J M. Graphite oxide flame-retardant polymer nanocomposites. *ACS Applied Materials & Interfaces*, 2009, 1(10): 2256–2261